nature communications

Article

https://doi.org/10.1038/s41467-025-66232-7

Vacuum-gap electrostatic multilayer actuators for space robotics

Received: 7 March 2025

Accepted: 3 November 2025

Published online: 11 December 2025

Check for updates

Ion-Dan Sîrbu[1,2], Arianna Mazzotta[3], Ubaldo Tosi[1], Daniele Bortoluzzi[4,5], Virgilio Mattoli[3], Giacomo Moretti[4] & Marco Fontana[1,2]

Actuation of space robots poses significant challenges in ensuring operation in vacuum. Conventional electromagnetic technologies face inherent limitations due to heat dissipation and difficulties in lubrication, whereas recent electrostatic alternatives, such as dielectric elastomer actuators struggle to reach their potential due to low reliability and lack of space compatible materials. Here, we introduce a class of electrostatic actuators that leverage the dielectric properties of the vacuum environment and turn it from a limiting factor into a key enabler. These devices rely on dielectric/conductive multilayer thin-film polymeric structures that enclose vacuum gaps, which unimpededly change in volume upon electrical activation, enabling zipping-like motions and generating actuation. Specifically, we demonstrate 0.7 g actuators delivering millimeter-range strokes, forces over 4 N, > 100 Hz bandwidth, and peak power-to-mass ratios of 1.4 kW kg^{-1}. Made from standard space polymers, they enable stackable, power-dense direct-drive actuation in vacuum environments, offering a promising solution for future space applications.

Space endeavours are imperative to the technological, scientific, and social flourishing of humankind. Their advancement heavily relies on inherently complex mechatronic systems designed to overcome extraordinary environmental and logistical limitations[1]. Actuation, either autonomous or remotely operated, is one of the main criticalities of such systems. It must execute diverse, yet often highly specialized tasks, such as operating deployable structures and spacecraft appendages[2], engaging optical instruments[3], operating launch lock and release mechanisms[4], spacecraft control systems[5], enabling on-orbit servicing strategies[6] and exploratory robots on celestial bodies— through robot locomotion, sample retrieval, manipulation, and analysis[7,8]. Typical spacecraft components must operate efficiently at extreme temperatures (typically −60 to +95 °C)[9] and low pressures with minimal outgassing, be resistant to ionizing radiation and corrosion[10], withstand shocks during launch[11], and in particular cases, cope with dust accumulation on planetary missions or provide high accuracy for communication or optical instruments.

For many such tasks, space missions typically employ electromagnetic actuators, often stepper or brushless DC motors[11,12], due to proven reliability, sturdiness, good performance in terms of accuracy, repeatability, and lifetime. Nevertheless, for efficient force/torque delivery, these are equipped with mechanical transmissions, which significantly increase mass, volume, complexity, cost, and demand lubrication[7,13,14]. This adds the need for thermal regulation solutions, either to heat up the system to avoid freezing of the lubricants at low temperatures, e.g., for missions on the dark side of the Moon or in deep space[13], or to cool it down to avoid overheating due to the lack of convection in vacuum, which can lead to catastrophic failures through mechanical seizing, short-circuits or even loss of magnetization[15]. Furthermore, the electromagnetic drives lose efficiency at lower dimensional scales (several centimetres and below)[16], making them less suitable for many recent efforts in the miniaturization of space technologies, such as the smallsats, where both the available space and power are highly limited[17].

[1]Institute of Mechanical Intelligence, Scuola Superiore Sant'Anna, Pisa, Italy. [2]Department of Excellence in Robotics & AI, Scuola Superiore Sant'Anna, Pisa, Italy. [3]Center for Materials Interfaces, Istituto Italiano di Tecnologia, Pontedera, Italy. [4]Department of Industrial Engineering, University of Trento, Trento, Italy. [5]Italian National Institute for Nuclear Physics (INFN), Rome, Italy. e-mail: marco.fontana@santannapisa.it

Smart material actuators are possible alternatives that can tackle such challenges through lower complexity and costs, dimensional scalability, efficiency and power density[18]. Among these, piezoelectric actuators are space-qualified and often serve in applications where high resolution and precision and/or high response speeds are required, such as fine-tuning optical instrumentation, active vibration damping, or engaging release mechanisms[3,17,19–22]. However, piezoelectric actuators are limited by very low actuation strains, typically well under one percent[15,23]. Shape memory materials (SMMs), on the other hand, achieve high strains, but with reduced strain rates and short lifespan. Although SMMs can be relevant for slow dynamics applications, such as low-shock release and latching mechanisms[24], deployable[25] or shape morphing structures[26], their thermal control is difficult in environments with extreme temperature fluctuations.

In this context, electrostatic actuation can be a groundbreaking technology, as it provides large strokes within wide frequency ranges, low power consumption, a lightweight structure, virtually unaffected by temperature variations, and lacks friction and its associated heat and lubrication challenges[27]. On Earth, variable capacitance actuators employing air as the dielectric have traditionally been confined to small-scale applications, such as microelectromechanical systems for sensing applications or for submillimetre scale position tuning. At larger scales, higher dielectric strength materials must be utilized instead of air, because its breakdown strength is a function of the dimensional scale (Paschen's law), with microscopic air gaps sustaining orders of magnitude higher electric fields than macroscopic ones. This prompted the development of dielectric elastomer actuators (DEAs), which employ the electrostatic deformation of soft elastomeric membranes to achieve displacements ranging from 10^{-4} to 10^{-1} m, with strains over 100%[28] and generated forces between 10^{-1} and 10^{2} N. Despite this potential, DEA technology is still at a pre-commercial stage. A major factor that hindered their expansion is their sensitivity to dielectric breakdown, which restricts the maximum electric fields that can be reliably and continuously applied, hence limiting their force and power density. Moreover, the narrow choice of space-compatible elastomers of just a couple of polydimethylsiloxanes (PDMS)[29,30] is also a concern. Therefore, investigations of their employment in space are limited to a few conceptual proposals of inflatable structures[16,31], space mirrors[32], mechanisms for regolith transport[33,34] and grippers[35].

A previous work that primarily targeted large actuated space structures attempted flexible electrostatic bending actuators, but was hindered by breakdowns and fast polymer charging due to using air as dielectric[36]. Recent developments in the field of soft robotics however - the electrostatic multilayer systems (EMSs) - use variable-thickness gaps containing insulating liquids instead of air, enclosed within flexible polymeric shells[37]. Some notable architectures, such as the hydraulically amplified self-healing electrostatic (HASEL) actuators[38–40], rely on the encapsulation and Maxwell pressurization of incompressible dielectric liquids, which can generate sealing and cavitation challenges in space, hence making this design unsuitable for such applications. Conversely, some other EMSs, mainly the electrostatic bellow muscles (EBMs)[41] and Electro-Ribbon actuators[42], can potentially operate without incompressible liquids, by utilizing other high dielectric strength media, such as a high vacuum, offering a promising solution for space applications.

Herein, we report an electrostatic actuation principle that treats vacuum not as a hindrance, but as a key functional asset, enabling operation in low-pressure environments. Our solution does not suffer from the heat transfer limitations and the complexity associated with electromagnetic drives and achieves significantly reduced mass and volume if compared to other electrostatic actuators due to employing vacuum as the bulk dielectric, as opposed to an elastomer or a liquid. Moreover, it is fully made of common space materials, such as polyimide (PI), whose dielectric strength we investigated under selected environmental hazards. The proposed vacuum-gap EMSs (V-EMSs) are intended to operate at pressures which cannot easily sustain gas ionization and corona discharges (well-below ~10^{-2} mbar). We demonstrate this promising direction by building actuators based on the zipping EBM principle, designed to operate in vacuum, and evaluate their performance in a vacuum testing chamber able to reach pressures on the order of 10^{-5} to 10^{-6} mbar. These devices can deliver comparable contractile strains to their liquid-based EBM counterparts (~40%)[41], but at larger strain rates (25,000% s^{-1}) and greater power density (1.4 kW kg^{-1}). Motivated by potential space applications, this work focuses on the evaluation of V-EMSs in vacuum condition.

We showcase this actuation method by developing a compliant gripper driven by a stacked EBM actuator, with the purpose of replicating object manipulation tasks representative of an idealized space mission. The gripper successfully grasps small objects inside our vacuum setup, demonstrating that vacuum-gap actuators based on thin and flexible materials and flexible structures, featuring stackable architecture, can be a promising option for low-pressure environments.

Results

General architecture and working principle of a V-EMS

Typical EMSs employ at least two dielectric media: solids, in the form of thin compliant polymer films, and liquids with low electrical conductivity and preferably low viscosity. Some actuator kinematics, such as in the HASEL actuator group[43], employ the liquid component in a dual role: (1) it must sustain sufficiently high electric fields required for the actuation to occur, hence an electrostatic functionality[44]; (2) it must deform the overall soft body of the actuator by means of pressurization and as a result, produce a mechanical movement, hence a hydraulic functionality. The combined electrohydraulic action demands both incompressible and high dielectric strength liquids. On the other hand, several other EMSs involve only an electrostatic action[41,42], enabling actuation solely based on the shrinking of the dielectric gap, whereas any pressurization of their liquids is merely a by-product of this process. This category does not necessarily require tightly sealed incompressible liquids and can enable the implementation of other dielectric media in the gap.

In view of this distinction, we propose an electrostatic actuation approach that employs a vacuum gap as one of the dielectric layers. High, ultra-high, and extreme-high vacua (pressures below 10^{-3} mbar) can represent optimal solutions in terms of dielectric strength and electrical conductive losses, as well as by providing negligible drag and no viscous resistance.

The envisaged fundamental structure of V-EMSs consists of two polymeric films separated by a vacuum gap, each carrying compliant electrodes on its outer surfaces (Fig. 1a). Upon the application of a voltage, the Coulomb attraction developed between the charged electrodes compresses the dielectrics and closes the gap, reducing the overall dielectric thickness to that of the films. To enhance protection from electrical discharges, the electrodes can be coated with thin non-conductive layers[45]. During the initial feasibility trials, we observed that such a thin protective coating significantly reduces the chance of vacuum arcs and enhances lifetime, especially during fast voltage transients or in proximity to grounded conductive materials. Furthermore, the proposed architecture can operate by electrostatic zipping, an actuation kinematics that relies on a spatially varying dielectric gap with minimum dielectric thickness at a contact front between the two films (Fig. 1a, b). This configuration concentrates the electric field in that contact region, lowering the required voltage compared to designs with spatially uniform gaps. The progressive closure of the gap mitigates pull-in instability effects, thus allowing more control over the actuation[42,43,46]. Similar to liquid-based devices, V-EMSs can utilize highly electrically resistive dielectric materials. Although they require voltages on the order of kilovolts, the associated

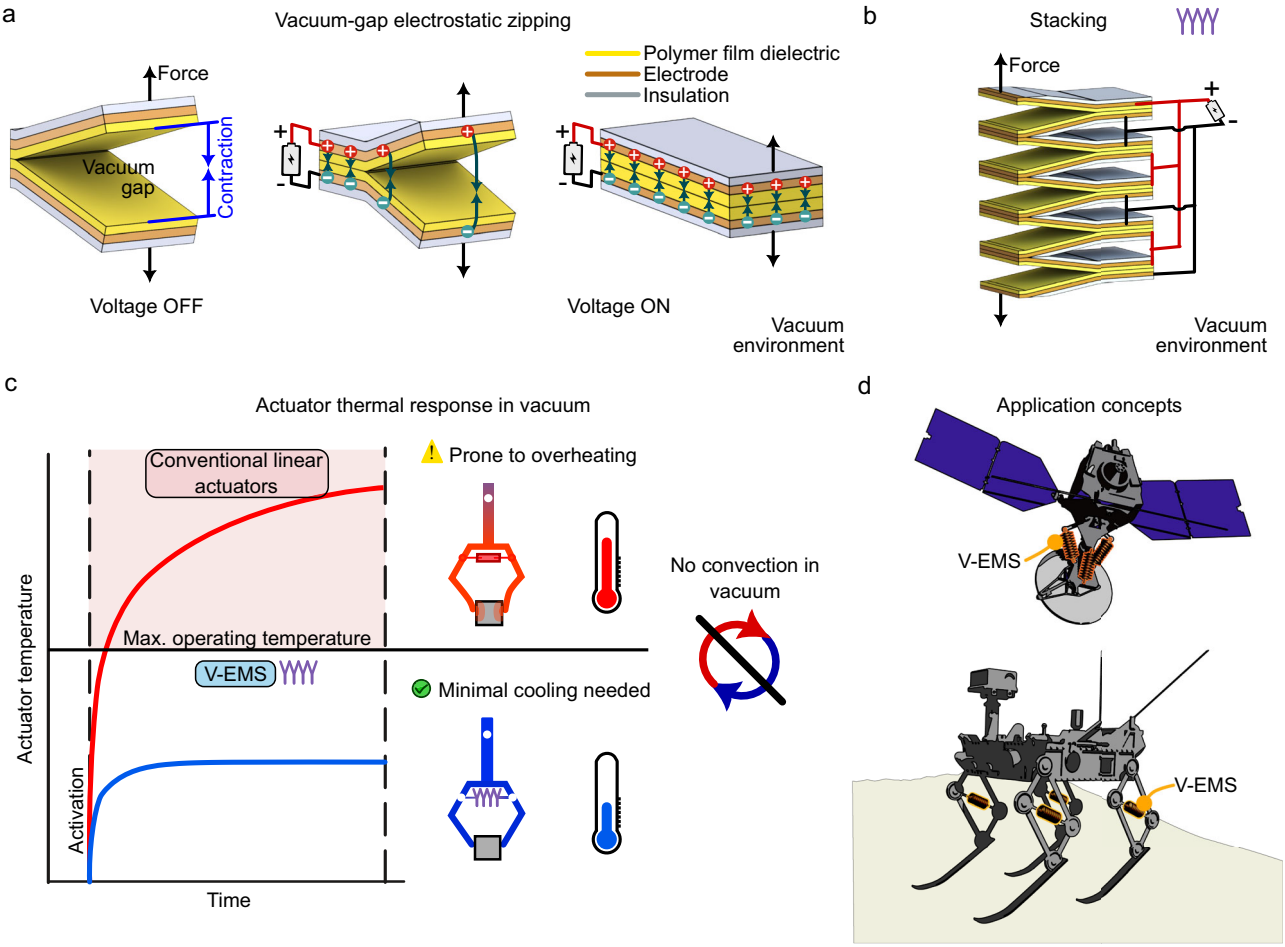

Fig. 1 | Key aspects of V-EMS. a General schematic of the working principle and kinematics of a zipping joint in vacuum. This zipping principle can be used to achieve stroke generation through different actuator configurations, leveraging a progressive contact of the polymeric films against an external force. *Left*: In deactivated state, the two films take a wedge-like profile, with the thickness of the vacuum gap being close to zero at the contact between the films, and very large on the opposing side. *Middle*: Upon electrical activation, the Coulomb attraction generated between the charged electrodes gradually brings together the films, closing the gap. *Right*: The polymer films come in full contact and full contraction is achieved. **b** Multiple zipping units can be integrated to increase performance. This picture presents a stacked configuration of a generic set of zipping elements, in which the actuation stroke is amplified proportionally to the number of units. **c** A schematic comparison of thermal behavior in vacuum: conventional actuators often require dedicated thermal management, while the proposed electrostatic actuators exhibit minimal self-heating. **d** Artistic representations of future applications of multilayer zipping joints onto space robotic systems.

currents remain extremely low, which results in minimal energy dissipation and limited temperature increase (Fig. 1c), which is a critical trait for vacuum environments. This behavior is demonstrated in the Section Temperature response during operation in vacuum.

The fundamental reliance of the V-EMS principle on a vacuum medium highlights a potential for driving mechanical structures in space (conceptually depicted in Fig. 1d).

The vacuum-gap EBM layout and working principle

To validate the feasibility of V-EMSs in a vacuum, we opted for the EBM as a proof-of-concept due to its straightforward and robust design, geometrical compatibility with our vacuum hardware and available fabrication know-how. The EBM is a versatile, easily-stackable contractile actuator, initially proposed as an artificial muscle for soft robotics applications in 2021[41].

First, we built a vacuum-gap EBM (V-EBM) stack consisting of three units connected in series, which we refer to as the preliminary V-EBM prototype throughout the remainder of the manuscript. Each unit contains two Polyimide (PI) dielectric films, bonded together on a circular perimeter and radially constrained by two rigid annular frames (Fig. 2a). The units are equipped with thin metallic electrodes with a diameter of 30 mm, that compress the dielectric when charged. To prevent electrical discharges, the V-EBM is fully coated with a thin layer of Parylene C. Critically, each unit is equipped with coaxial needle-size vent holes for air evacuation during depressurization and establishment of equilibrium between the internal volume of the device and the vacuum environment. In contrast to literature, this device lacks dielectric liquids and their related storage and filling components; hence, it has a mass of 5.3 g, almost half that of a liquid-based device with polymer frames.

When a tensile force is applied to the actuator, its thin, polymeric structure elongates and the two PI films in each unit gradually separate and form gaps between them. When a sufficiently high voltage is supplied, electrostatic attraction between the electrodes drives the films back together in a zipping motion, closing the gaps and producing a contraction of the units as illustrated in Fig. 2b.

Upon dimensional scaling, the key actuation parameters, such as stroke and energy density, exhibit predictable trends. In liquid-based EBMs, the stroke scales up with radial dimensions, assuming that the electric field is maintained, but the energy density decreases, since the mass, dominated by the liquid, grows cubically[41]. In a vacuum device though, the stroke will scale in the same way, but, critically, the energy

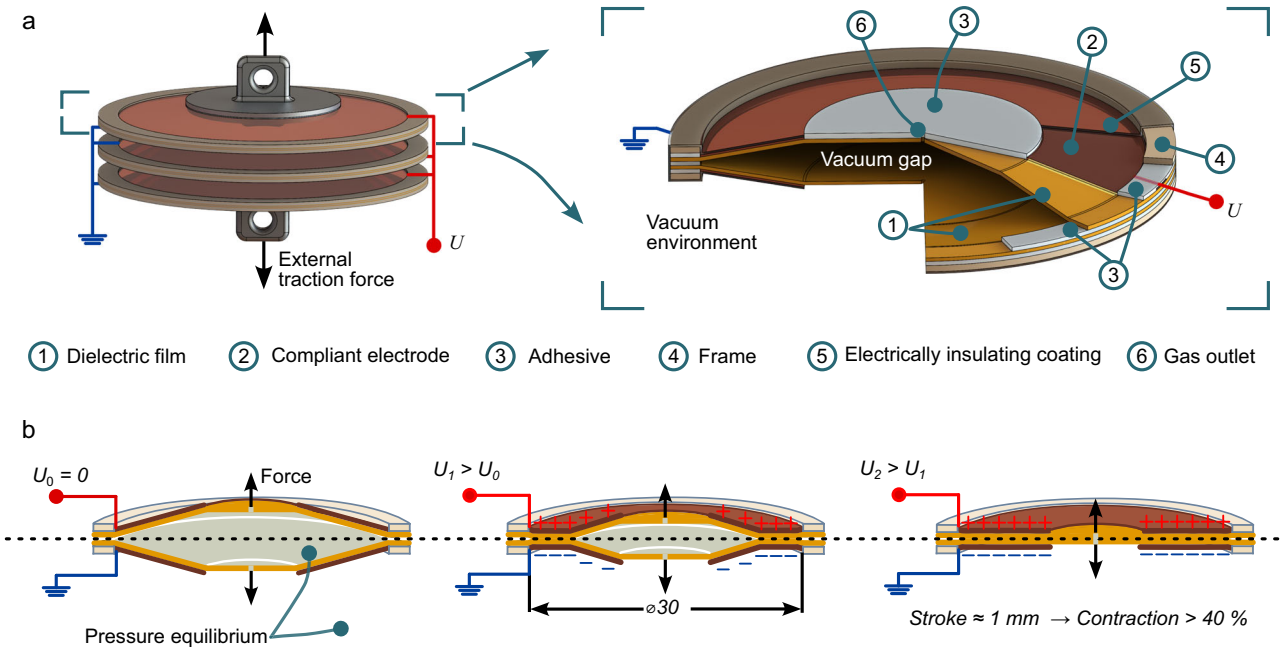

Fig. 2 | V-EBM structure and working principle. a Rendered view of a stack and structure of each actuation unit subject to an external traction force and a voltage *U*. **b.** The zipping kinematics of the actuator. At no applied voltage, the device is stretched by the external force and the gap is at its largest. With the increase in voltage, the polymer films gradually come in contact, reducing the gap.

density will remain constant within large dimensional variations (Supplementary Information Section 5).

Although full space qualification is beyond the scope of this work, the intended future use of these actuators in space motivates investigations beyond vacuum compliance. To evaluate the electrical limits in response to selected environmental hazards representative for space, we performed a dielectric characterization of our PI material both as a function of temperature up to 145 °C, as well as of gamma radiation up to a dose as high as 1475 kGy (Supplementary Table 2). In both cases, the dielectric strength stayed significantly above the maximum electric field strength we deemed necessary to operate the V-EBM (~120 V/µm), with median breakdown values at least twice the necessary threshold. More details about these materials tests are available in the Supplementary Information Section 2 and Supplementary Fig. 2.

Characterization of the preliminary V-EBM

The characterization of the preliminary V-EBM was performed in a custom test bench integrated into a vacuum chamber equipped with a transparent vacuum dome for actuation monitoring (Fig. 3a and Supplementary Fig. 4). The experimental campaign was performed at pressures ranging from 5×10^{-5} down to 10^{-6} mbar. We investigated the maximum operational pressure threshold of the V-EBM in our vacuum system and identified it to be at around 10^{-2} mbar (Supplementary Fig. 1 and Supplementary Information Section 1). Above this limit, a critical pressure range for electrical breakdown begins, thus making V-EMS high voltage activation unsustainable. Therefore, for the characterization, we chose a pressure interval significantly below this value. The lower threshold of the chosen range is restricted by the pumping power of our vacuum equipment; ideally, the lower these pressure values, the less likely electrical discharges in the residual gas are to occur.

We applied voltages of 4, 5, and 6 kV, corresponding to electric fields of 80, 100, and 120 V µm^{-1}. The maximum applied voltage of 6 kV during characterization does not exceed 50% of the measured dielectric strength of the two PI films (Supplementary Fig. 2). We applied a switching sinusoidal voltage (Fig. 3b) by swapping the positive voltage terminal across the actuator each cycle, that allows applying bipolar sinusoidal voltage across the actuator while using only positive supply voltages, such as in refs. 47,48 (Supplementary Information Section 8). The switching is necessary as we noticed that applying DC voltage will otherwise introduce temporal changes in the output force of the actuator that are reminiscent of the interfacial charge accumulation in the dielectrics of liquid-based EMSs[37]. In fact, for the latter, a switching driving voltage is common practice to avoid detrimental charge accumulation within the dielectric layout, which significantly alters their force output. In the case of V-EMSs, such effects may stem from charge traps at the dielectric films' interfaces or within their bulk.

To determine the force-stroke characteristic, we applied voltage to generate actuation at a frequency of 5 Hz, while progressively increasing the mechanical loading of the device from 1 to 4.25 N. The loading was done by applying a slowly growing force ramp via a soft metallic spring (Supplementary Fig. 4) at a rate of ~0.06 N s^{-1}. The very slow rate ensured that the applied force is quasistatic during each actuation cycle and allowed a continuous force-stroke characteristic on the entire applied force range. We define the term elongation as the instantaneous position of the actuator, measured in millimeters relative to its fully contracted state (set as zero). Consequently, actuation stroke is the difference between the maximum and minimum elongation within each cycle.

Figure 3b illustrates a snippet of the elongation of the device during high voltage excitation, whereas Fig. 3c plots the actuator stroke during the entire force ramp. This device exhibited a blocked force close to 4 N at the maximum applied voltage of 6 kV, which decreased to 3 and 2.2 N at 5 and 4 kV, respectively (Fig. 3c). As expected, the stroke is highest at a relatively low preload of 1 N, reaching a maximum 3.6 mm, which corresponds to a contraction value close to 50% (Supplementary Figs. 9 and 10). This is higher by about 20% than in an equivalent liquid-based EBM, which must incorporate dedicated components to store the displaced liquid during actuation. This increases device size without adding any contribution to the overall deformation. Conversely, the functional vacuum dielectric eliminates the need for such structures, enabling V-EBMs to

https://doi.org/10.1038/s41467-025-66232-7

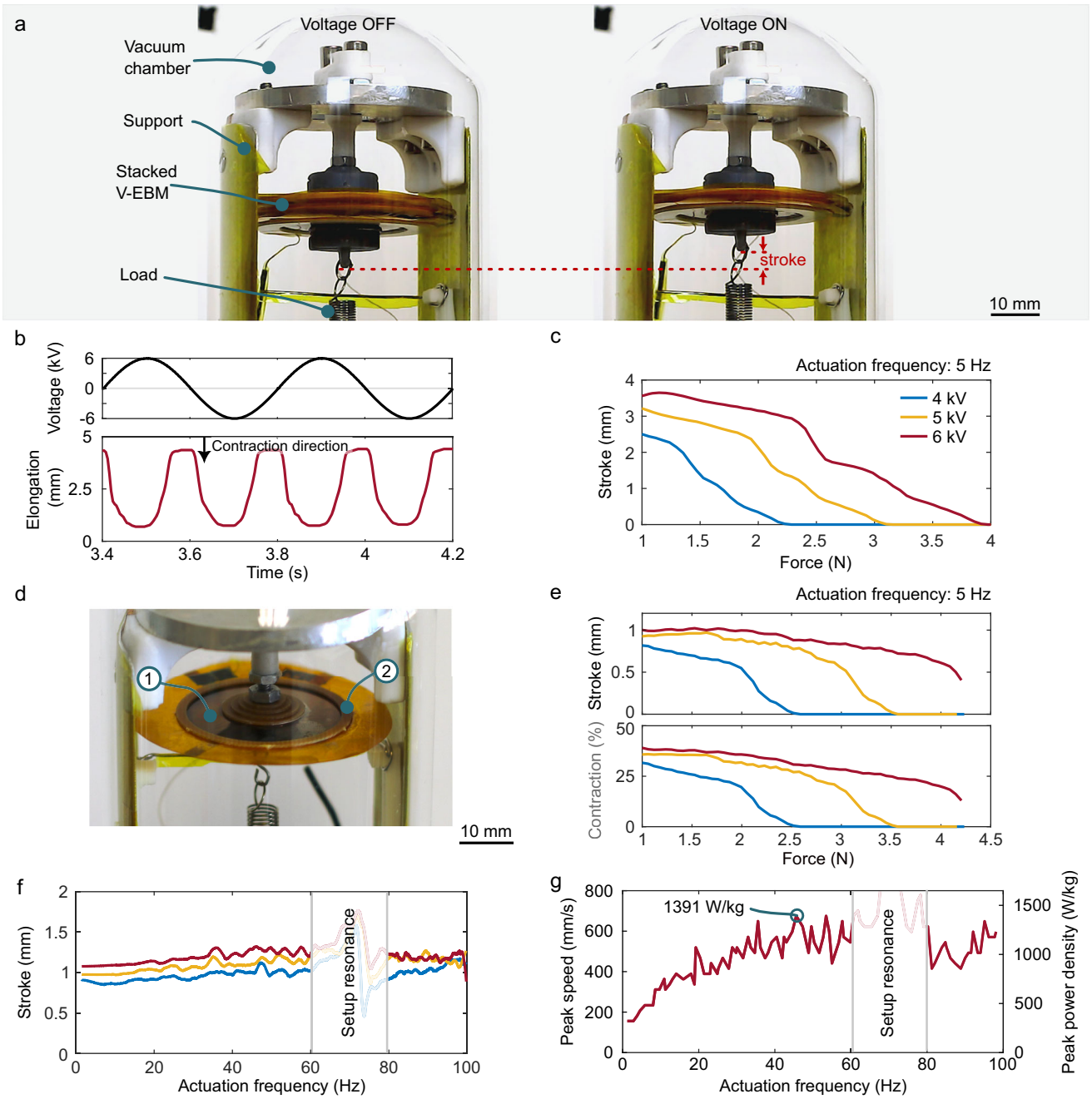

Fig. 3 | Characterization of the V-EBM. a Three-unit V-EBM stack actuating inside the vacuum chamber. **b** The real-time elongation (bottom plot) of the stack in response to being stretched by a force of -1 N and the applied voltage across the actuator (top plot). **c** The force-stroke behavior of the stack under 4, 5 and 6 kV excitation at 5 Hz actuation frequency. **d** Single-unit V-EBM optimized in terms of employing space-grade materials and having significantly reduced mass. Point ① marks the electrically active region determined by the electrode surface. Point ② indicates the narrow PI-laminate frames. **e** Force-stroke characteristic at 5 Hz actuation frequency of the single-unit V-EBM device (top plot) and its corresponding contraction-force dynamics (bottom plot). **f** Stroke as a function of actuation frequency of the single-unit V-EBM subjected to a 1.5 N load. All three applied voltages indicate comparable strokes at 1 and 100 Hz. The frequency region around 70 Hz corresponds to an instrumental resonance of the setup and is therefore excluded from performance estimations. **g** Peak speed and peak power-to-mass ratio as functions of the actuation frequency for the 6 kV dataset shown in (**f**).

make much more efficient use of their volume. Furthermore, the characterization revealed that the force and stroke output are comparable to the liquid-based EBM, but at less than half the actuator mass.

Characterization of an optimized vacuum-EBM

Following concept validation, we developed a lightweight single-unit V-EBM optimized in terms of employing high-temperature and low-outgassing adhesives, and refined frames made of a high-performance PI-fiberglass laminate, hereafter referred to as the optimized V-EBM. The materials employed in this version of the actuator have been previously implemented in space missions. A discussion of these materials can be found in the Supplementary Information Section 2, whereas the fabrication method is detailed in Materials and Methods and Supplementary Fig. 3. Besides space compatibility, the refinements in materials allowed a significant mass reduction of a unit down to just 0.7 g, which is roughly 1/9 the mass of an equivalent liquid-based device.

Despite being significantly lighter, the actuator exhibited a blocked force surpassing 4.25 N at 6 kV, more than 600 times its own weight on Earth, a stroke of 1 mm, and reached contractions of 40% (Fig. 3e and Supplementary Fig. 11), orders of magnitude higher than piezoelectric actuators, and comparable to silicone-based DEAs. Surprisingly, this optimized V-EBM demonstrated an actuation bandwidth greater than 100 Hz (Fig. 3f, Supplementary Fig. 12, and Supplementary Movie 1). However, this value must be considered as a conservative maximum, because the resolution of our measurement setup did not allow testing higher frequencies (Materials and Methods). The amplified oscillatory regime visible in the interval of ~60 to 80 Hz is not caused by the actuator, but by external disturbances imposed by longitudinal vibration modes of the preloading spring, which passes through its first natural frequency at around 72 Hz (estimation in the Supplementary Information Section 8), and which is connected in series to the actuator (Supplementary Fig. 4). Nevertheless, after this region, in the interval 80 to 100 Hz, the actuation stroke stabilizes and remains close to the one at lower frequencies, in the range close to 1 mm at both 5 and 6 kV. Furthermore, V-EBM can also operate at frequencies below 1 Hz, down to at least as low as 0.1 Hz (Supplementary Fig. 13 and Supplementary Movie 2), albeit polarity switching is still required to redistribute any accumulated charges within the dielectrics. This actuation frequency range can be useful both in dynamic tasks, like rapid tuning of optical or communication instruments and adjusting deployable structures, activation of valves, switches, latches, as well as in more general tasks, like driving scientific instruments, robotic manipulation, and others.

The actuator was capable of reaching a peak linear speed of 670 mm s^{-1}, corresponding to a contraction rate of 25,000% s^{-1} (piezo about 10,000% s^{-1}) (Supplementary Fig. 14). Furthermore, we estimated a maximum average power of 370 mW at around 100 Hz (Supplementary Figs. 15 and 16). The peak power, however, is close to 1 W, resulting in a peak power-to-mass ratio of 1.4 kW kg^{-1} (Fig. 3g), and a peak power-to-volume of 0.9 MW m^{-3}, calculated considering a device cylindrical envelope of ~1.09 cm^3 (Supplementary Information Section 4). The unit operated for a minimum of 500,000 cycles at 4 kV (Supplementary Fig. 17), despite suffering some damage to the protective coating over time.

Temperature response during operation in vacuum

Equipment overheating is a primary concern in low-pressure environments due to the lack of convective heat transfer. To avoid failure, actuators in space are typically endowed with thermal management and monitoring solutions that inevitably increase system complexity and power consumption. Therefore, the evaluation of the thermal response of the proposed electrostatic actuators in vacuum is of paramount importance.

While in theory electrostatic actuators might retain their stroke against an applied force with no power consumption, in practice leakage currents due to the dielectrics' conductivity are a source of heat generation. In a fully zipped actuator, Joule power losses can be thus estimated to be proportional to the squared applied voltage, the polymer conductivity, the electrodes' surface area, and the inverse of the total dielectric thickness (Eq. S5). Given that the conductivity of the PI used in this work is on the order of 10^{-15} S m^{-1}[37], the dissipated power per unit device mass, in a zipped state, can be calculated on the order of 1 μW g^{-1}. Despite just representing an order of magnitude, this estimate falls several orders of magnitude below the dissipated power density of electromagnetic drives, e.g., typical brushless DC motors, whose losses can be estimated within the range of a few tens of mW g^{-1}. Under fast switching voltage though, electrode resistance might become a bottleneck. Nevertheless, even with the conservative assumption of an equivalent electrode resistance on the kΩ order and high frequency operation, the power loss is expected to be significantly less than that of electromagnetic motors (see the heat dissipation considerations in Supplementary Information Section 9 and Supplementary Table 3).

Based on these considerations, we carried out experiments to measure the temperature variation of the optimized V-EBM during actuation with a high-resolution infrared (IR) camera. The IR transmission from the device inside the vacuum chamber to the camera outside is ensured by a dedicated IR-transparent viewport. To minimize the conductive heat transfer between the actuator and the setup, the mechanical contact is reduced to the electrical connection, and to the support and loading points (made of PI laminate in our setup), all of which are unavoidable regardless of the implementation. Furthermore, although coated with Parylene C, the surface of the V-EBM is highly reflective to IR radiation, a problem that we solved by applying on the actuator small PI thermal markers with high emissivity coefficients, thus enabling IR-based temperature readings without impeding actuation. This setup is described in more detail in Materials and Methods and Supplementary Fig. 5.

The actuator is subjected to a load of 1 N in all the temperature tests. To determine the temperature increase arising from dielectric conductive losses, we applied a 60 s 4 kV DC signal. In the case of dynamic modes, in which the losses from electrode heating become dominant, the thermal response was assessed by subjecting the actuator to a 4 kV switching voltage at 1, 10 and 50 Hz for 60 s. Remarkably, the device does not show any temperature increase neither during DC nor at 1 Hz operation, whereas it manifests a minor rise of less than 0.5 °C at 10 Hz and a mere 2 °C at 50 Hz (Fig. 4a).

Moreover, we also tested the most dissipative scenario of high-frequency 100 Hz actuation for longer periods of time −600 s, and at higher voltage −5 kV, as well as at 4 kV. The results demonstrate a temperature increase of about 6 °C and 7.5 °C for 4 and 5 kV, respectively (Fig. 4a, b), both cases producing a thermal time constant in the range of 100 s. Therefore, the V-EBM manifests trivial temperature changes during actuation and small variations between the applied voltage amplitudes and frequencies. Additionally, the geometry of these actuators allows a very large surface-to-mass ratio of more than 2.7 m^2 kg^{-1}, in the range of lightweight radiators for CubeSats.

Gripper demonstrator

To explore the potential of integration of the V-EMS technology with external mechanisms, we developed a compliant mechanism gripper driven by a three-unit V-EBM. This serves as a conceptual application example, that the actuator's performance in terms of stroke (and stacking) and actuation speeds can be well-matched to a relevant tool for space robotics. The gripper features a minimalist monolithic structure and operates as a distributed compliance mechanism through a set of thin interconnected cantilever springs (Fig. 5a). Besides implementing the gripping kinematics, this mechanism performs a secondary role of providing the preliminary V-EBM stack with the pre-stretch required for operation (2–3 mm) (Supplementary Fig. 18). Moreover, the gripper also amplifies the stroke of the actuator, converting it into a displacement between fingertips that is ~6 times greater.

The resulting device is capable of grasping objects in low-pressure environments. Figure 5b and Supplementary Movie 3 show the gripper handling an 8.6 g rock inside the vacuum chamber at a pressure of ~10^{-5} mbar, simulating a robotic mission for the collection of rock samples. Initially, the V-EBM is extended, and the gripper is open. We then apply high voltage, causing the actuator to contract and the gripper to pinch the rock. The gripper is then pulled upwards by a motorized testbench (Supplementary Fig. 6), whilst firmly holding the rock suspended. Because the experiments were brief, charge accumulation effects did not manifest disruptive contributions to the force output of the actuator and did not impede the grasping process as a whole, hence, it was possible to perform them at 6 kV DC.

https://doi.org/10.1038/s41467-025-66232-7

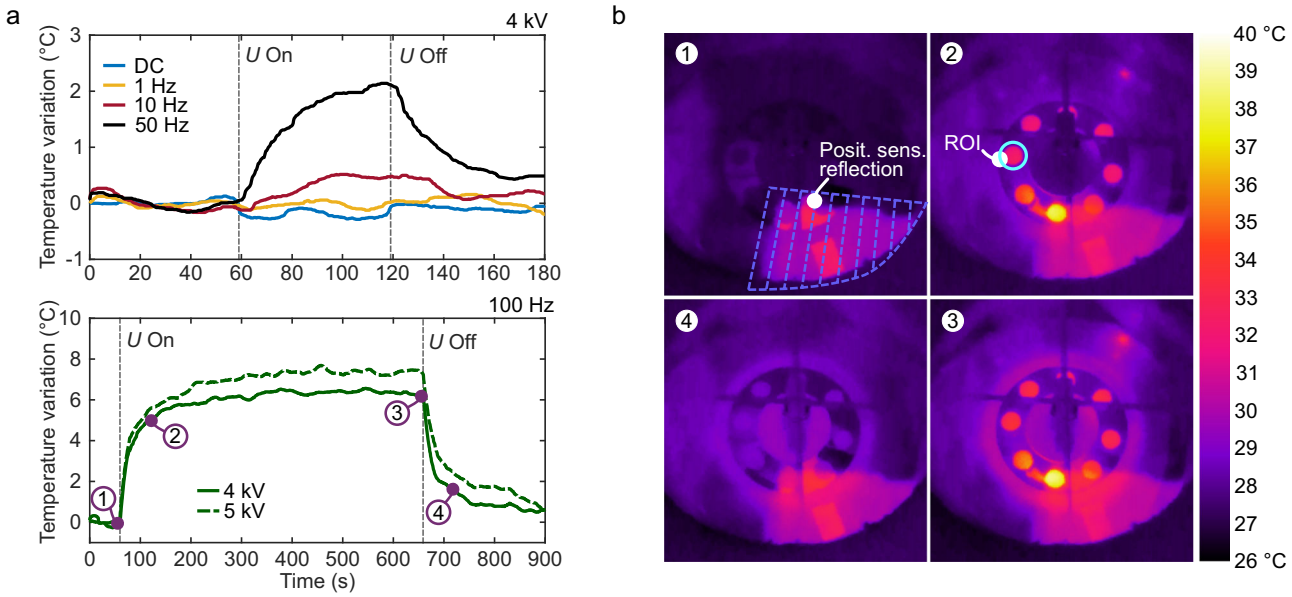

Fig. 4 | Temperature variation of the V-EBM during actuation. a Graphs showing the measured thermal response of single-unit V-EBM with a preload of 1 N, during: (top) 60 s actuation tests at a voltage U of 4 kV - either DC, or under switching sine signal of 1, 10 and 50 Hz actuation frequency, and (bottom) 600 s actuation tests at the most dissipative scenario of 100 Hz at 4 and 5 kV. **b** Thermal images taken during the 100 Hz 4 kV test in the instances indicated in the panel a. Frame ① indicates the initial thermal state immediately before the voltage was switched on, frame ② - the voltage was activated for 60 s, frame ③ - voltage activated for 600 s and frame ④ - voltage was switched off for 60 s. The reflection of the position sensor employed to confirm actuation is covering the lower right portion of each frame, visible as a hotter triangular region (hatched area) and was discarded in temperature estimates. The temperature was extracted as the maximum value on the region of interest (ROI) indicated in frame ②, free from significant reflections and corresponding to one of the 10 PI markers.

This process was repeated with a 3.6 g aluminum cylinder, representative, for example, of a small satellite component to be grasped (Supplementary Movie 3). Additional performance details about the gripper-EBM system can be found in the Supplementary Information Section 10. The mass of the grasped objects and the overall performance of the system can be further improved by tuning the compliance of the gripper mechanism and the dimensions of the EBM actuator.

Discussion

Here, we introduce V-EMS, a class of actuators that exploit unique properties of vacuum - namely its high dielectric strength and resistivity, and lack of viscosity - to deliver large strokes and forces at short response times. In our proposed approach, a wide vacuum gap between two flexible polymer films forms highly contractible dielectric structures that change their shape when electrostatically pressurized by compliant electrodes. Unlike conventional actuators for space, which often regard vacuum as a technological hindrance (for example, causing overheating in electromagnetic actuators), our approach exploits vacuum to boost actuation performance by leveraging the large electric fields it can sustain, the low conductivity and the absence of fluid dynamic resistance during contraction. This enhances multiple performance metrics, such as mass, speed and power, compared to EMSs that use dielectric liquids on Earth.

To demonstrate this principle, we built actuator prototypes, called V-EBMs, and tested them in a low-pressure environment. Unlike conventional electromagnetic motors, such actuators are well-suited for centimeter and gram-scale applications. Furthermore, these actuators can be made of polymers commonly employed in space. In our implementation, we estimated the materials cost per actuation unit of an optimized V-EBM to be ≈ 2 €, although by scaling up fabrication this cost can be reduced even further. Even though further space qualification is required for the actuator as a whole, the materials cost is expected to remain low.

Such actuators were capable to pull loads higher than 4.25 N while having a mass of only 0.7 g and achieved a contraction rate of over 25,000% s^{-1} and a power-to-mass ratio of 1.4 kW kg^{-1}. Notably, they do not heat up significantly, even in the most demanding cases the measured temperature increase is as little as 7.5 °C. Furthermore, we integrated a stacked V-EBM in a compliant gripper mechanism and operated it in vacuum. Although this gripper is a conceptual demonstrator for operation in vacuum rather than an optimized and final space system, it successfully grasped small objects inside our setup.

The pressure range in which the experimental campaign was undertaken is 5×10^{-5} to 10^{-6} mbar. Pressures below this range might be beneficial because they further reduce the number of residual gas molecules, thereby minimizing ionization. At higher pressures, i.e., medium and rough vacuum, gas ionization is expected to hinder actuation (corona, arc discharges). Preliminary tests in our vacuum test bench showed that pressures above 10^{-2} mbar prevent actuation due to electrical discharge phenomena in the residual gas (Supplementary Fig. 1). Although more investigation regarding the V-EMS operation at such low vacuum levels is required, ceasing operation is recommended for low vacuum or transient pressures. Given that uncrewed spacecraft are typically unpressurized and operate in high vacuum conditions, our actuator demonstrates compatibility with environments inside such spacecraft in terms of pressure. While outgassing from the actuator materials was not quantitatively assessed, the use of common space polymers is expected to reduce contamination risks, and future material selection can be further optimized based on standardized outgassing metrics as mission requirements dictate[49]. Unlike DEAs, V-EMSs can effectively leverage a wide range of space-grade materials, with possible dielectric candidates, besides PI, being dielectric films of polytetrafluoroethylene (PTFE), Mylar, nylon, Parylene, etc. The selection will be tailored to mission-specific constraints, as relevant electrical and mechanical properties of polymers change with exposure to space hazards[50].

Although this work already demonstrates V-EMS in vacuum - serving as a proof of concept with consideration of relevant materials

https://doi.org/10.1038/s41467-025-66232-7

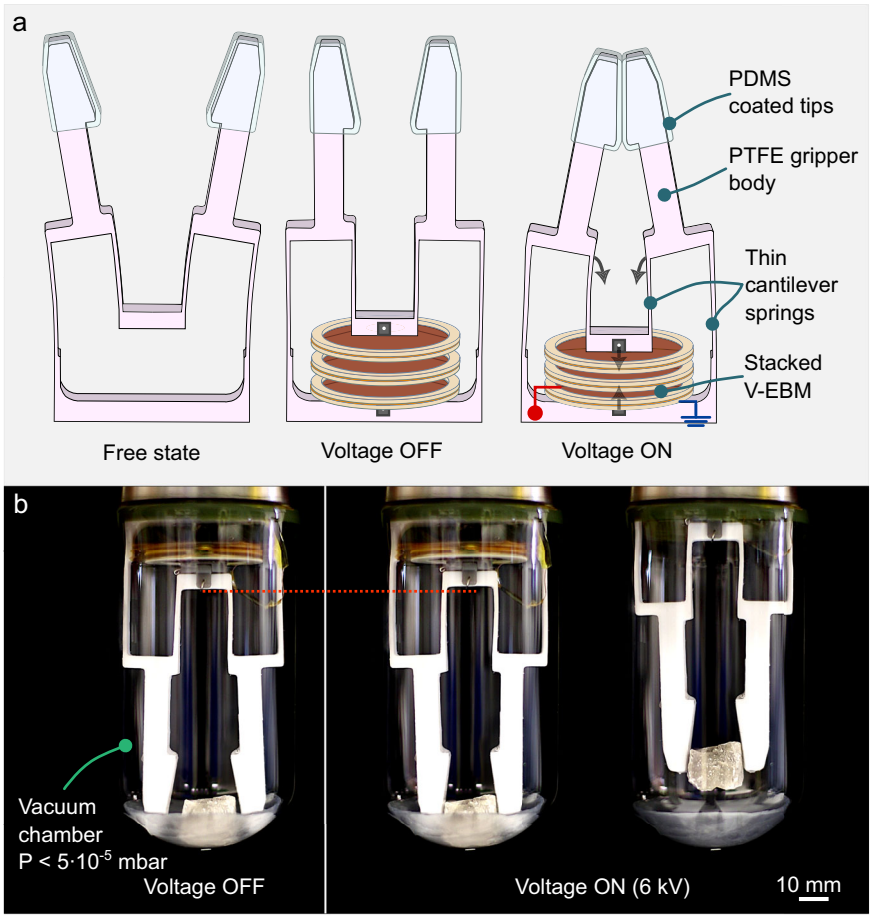

Fig. 5 | Compliant gripper demonstrator. a The actuation process of the gripper. Left to right: gripper in free state; gripper stretching the actuator when the latter is inactive; clamping action instigated by the electrical activation of the actuator. **b** Rock grasping demonstration in the vacuum chamber. Left to right: gripper is inactive; the contraction of the stacked V-EBM in response to a 6 kV DC high voltage signal causes the gripper to bend and grasp the rock; the activated gripper and the rock are lifted with the motorized test bench.

for space use, critical space-related aspects must be explored. Future studies must investigate long-term performance and electrical aging under real mission conditions, offer a more comprehensive assessment of resilience to space hazards, determine the response to mechanical shocks during launch, as well as investigate and develop integration methods with existing space platforms. Regarding the latter, there exist numerous space missions that already employ high voltage supplies for other tasks, such as propulsion, and operation of scientific instruments like spectroscopy analyzers, cameras, radars, travelling-wave tube amplifiers, etc[51–53]. Although systems integration and closed-loop control are steps yet to be taken, the know-how and possible synergies with established high-voltage space technologies might be a boost to drive space V-EMS to technological maturity. Therefore, this actuation solution could benefit from the expertise and interest regarding high-voltage supply and protection measures in space. Furthermore, dedicated control strategies are possible, likely based on self-sensing capacitive methods[39], for performing trajectory tracking, force control or other tasks, as well as for guaranteeing robustness against unpredictable external forces.

Future actuator geometries, materials solutions, and reliability assessments in task-oriented evaluations could determine the place for V-EMSs onboard space missions.

Methods

Preliminary V-EBM prototype

This actuator is a three-unit stack consisting of three identical actuation units mechanically connected in series and electrically in parallel. Each unit is made of two PI dielectric films (PIT1N, Caplinq), each 25 μm thick, bonded on a circular perimeter by a 5 μm thick double-sided annular adhesive strip (No. 5600, Nitto Denko), and constrained on an external circumference by two rigid annular frames. It bears two compliant 10 nm thick copper electrodes on its external surfaces (Fig. 2a), applied via DC metal sputtering (Q150T-ES, Quorum Technologies) on the PI films through a masking process prior to the actuator assembly. Each unit also holds two double-sided adhesive pads (VHB 4905P, 3M) on its external surfaces for bonding to the adjacent units or to the interface elements. The latter are small plastic parts designed to integrate the actuator into the test bench, and, in case of the EBM stack, are 3D printed (GreyPro, Formlabs). The frames are made of FR-4 epoxy resin and are attached to the PI substrates with 0.1 mm double-sided acrylic adhesive tape (68144, Tesa). Additionally, the units feature small coaxial vent holes that ensure pressure equilibrium between the internal volume of the device and the external vacuum environment during transients. The vents have a diameter of around 0.6 mm in the PI films, and 1 mm in the interface elements and adhesives. The external surface of the stack is fully coated with a 7 μm thick layer of Parylene C by placing the device in a parylene coater (PDS2010, Specialty Coating Systems) in which 4.8 g of Parylene C was loaded. Parylene C dimer was purchased from Specialty Coating System Inc. (IN, USA). During deposition, we cover the vent holes with a porous tissue such as to prevent material from entering inside the devices, while still allowing air venting in the initial stages of this process. More details about this can be found in the Supplementary Information Section 3.

Optimized V-EBM unit

This actuator consists of a single unit and employs materials with higher tolerance to space hazards. In this case, all mechanical bonds are realized with a high-temperature adhesive (Pyralux LF0100, DuPont). The frames feature a minimalist design and are made of a PI/glass fiber composite (85N Polyimide Laminate, Arlon). This material was also employed by the interfacial elements. The device consists of four materials: PI, copper, Parylene C and the LF adhesive.

The electrodes are identical in both actuators, with 16 mm internal and 30 mm external diameters. Supplementary Table 1 contains the exact dimensions of all the components of the two actuators. Further details about the materials, their use in space applications, the fabrication methods, actuators dimensions, mass and volume can be found in the Supplementary Information Section 4.

Gripper materials

The gripper is carved from a PTFE slab (RS Pro) with a desktop CNC machine (3018-PRO CNC, Gemnitsu). The fingertips are coated with PDMS (Sylgard 184, Dow) by dipping, to improve grip and compliance.

Vacuum setup

The test bench has at its core a turbomolecular pumping station (T-Station 85, Edwards), connected to a vacuum chamber of stainless steel (304/304L) flanges and tubes (Supplementary Fig. 2). The system is equipped with a glass vacuum dome, a pressure gauge (PBR260 or PKR251, Pfeiffer), a venting valve, a high voltage electrical feedthrough, and a motorized linear mechanical feedthrough. The latter conveys a linear motion, generated in the atmosphere by a motor, to the vacuum environment, with the scope of extending a soft spring (SODEMANN Industrial Springs) through which a tensile force is applied to the actuators (Supplementary Fig. 4). The spring approximately functions as a constant biasing force. It features a maximum elongation exceeding 100 mm - two orders of magnitude greater than the stroke of a single-unit EBM, and a very low stiffness - of just 0.032 N/mm. As a result, the variation in the applied force during actuator contraction can be considered negligible: a 1 mm stroke of the unit actuator results in a force change of only 0.032 N, which corresponds to an error of just 0.75% to 3.2% across the full range of applied forces (Supplementary Information Section 6).

Characterization process

The actuators are rigidly fixed, on one side, to a rigid non-anodized aluminum and PTFE support structure inside the glass dome, and on the other are connected to the spring. The feedthrough that stretches the spring and applies the load is actuated by a linear motor (L16-P, Actuonix) with calibrated position feedback, hence directly providing information on the spring elongation and allowing estimation of the applied force using Hooke's law. The experimental campaign is carried out at pressures ranging from 5×10^{-5} down to 10^{-6} mbar.

The driving voltage is supplied with two high voltage amplifiers (10HVA24, Ultravolt), which also provide current and voltage sensing capabilities. Each electrode is charged with a positive sinusoidal signal, then grounded, in alternating cycles depicted in Supplementary Fig. 8, such as to induce a switching voltage signal across the actuators (see Supplementary Information Section 8 for more details about the applied voltage). The characterization was performed at voltage amplitudes of 4, 5 and 6 kV.

The actuators are recorded through the glass dome with a high-speed camera (GS3-U3-23S6M-C with lens 250F6C, Point Grey). Each video frame is TTL triggered with a Speedgoat Baseline Real-Time Target machine, which also controls the linear motor through a PID controller, generates the driving signals for the amplifiers, and acquires the voltage, current, and pressure data. The actuator elongation is then estimated using Matlab video processing methods (Supplementary Fig. 7).

Force-stroke characterization

The stroke as a function of force is determined by subjecting the actuators to a force ramp from 1 to 4.25 N with a slope of ~0.06 N/s, while supplying voltages of 4, 5, or 6 kV amplitude and actuating at 5 Hz.

Frequency characterization

The optimized V-EBM is loaded with a constant force of 1.5 N and driven with a switching up-chirp signal either from 0.1 to 1 Hz for quasistatic tests (Supplementary Movie 1) or from 1 to 100 Hz for dynamic tests (Supplementary Movie 2) at 4, 5 and 6 kV.

Temperature response

The temperature measurements are performed on optimized V-EBMs. To reliably measure the temperature, 10 thin circular markers were attached to the Parylene-C coating, as depicted in Supplementary Fig. 5. Each marker has a diameter of 4 mm, a thickness of 110 µm and is made of three layers of PI - silicone adhesive tape (PIT05S by Caplinq). Two markers are placed on the electrical connection between the wires and the electrodes, and 8 are placed at equal angular intervals on the electrode monitored by the IR camera.

This optimized V-EBM is mounted inside a steel vacuum chamber and fixed at the top side on a support structure made of thin (0.5 mm) PI-fiberglass laminate beams. The IR camera (A70, with FOV 51° lens, FLIR) is mounted at ~20 cm above the actuator, such as to have a clear overview of its top surface. Also from the top, a laser meter (LK-G152, Keyence) is used to detect actuation by pointing towards the top annular frame. The laser produces a reflection that covers roughly 17% of the area of interest, which was not considered for results evaluation. The load is applied via a soft spring connected in series to a vacuum compliant load cell (KD24S 20N, ME-Meßsysteme) (Supplementary Fig. 5).

Gripper tests

The V-EBM stack is incorporated into the body of the compliant gripper, which is attached directly to the motorized feedthrough (Supplementary Fig. 6). The actuator is activated (6 kV DC) when the fingertips are in proximity to the object, hence grasping it. Subsequently, the motorized system lifts the gripper with the grasped object following a predetermined trajectory inside the vacuum setup (Fig. 5 and Supplementary Movie 3).

Data availability

All data are available in the main text or the supplementary materials.

References

1. Gao, Y. & Chien, S. Review on space robotics: toward top-level science through space exploration. *Sci. Robot.* **2**, eaan5074 (2017).
2. Duan, B., Zhang, Y. & Du, J. *Large Deployable Satellite Antennas: Design Theory, Methods and Applications* (Springer-Verlag, 2021).
3. Allegranza, C. et al. Actuators for space applications: state of the art and new technologies. In *Proc. 14th International Conference on New Actuators, Bremen, Germany*, 23–25 (Messe Bremen, 2014).
4. Berlin, M., Goossens, N., Oelze, H. W. & Braxmaier, C. Launch lock system for reaction wheels. *CEAS Space J.* **13**, 583–589 (2021).
5. Gilbertson, R. G. & Busch, J. D. A survey of micro-actuator technologies for future spacecraft missions. *JBIS* **49**, 129–138 (1996).
6. Flores-Abad, A., Ma, O., Pham, K. & Ulrich, S. A review of space robotics technologies for on-orbit servicing. *Prog. Aerosp. Sci.* **68**, 1–26 (2014).
7. Townsend, J. et al. Mars exploration rovers 2004–2013: Evolving operational tactics driven by aging robotic systems. In *Proc. 13th International Conference on Space Operations, SpaceOps* 2014, 1–22 (AIAA, 2014).

8. Matijevic, J. & Dewell, E. Anomaly recovery and the Mars Exploration Rovers. In *SpaceOps 2006 Conference*, 1–17 (AIAA, 2006).
9. Fortescue, Stark, P. J. & Swinerd, G. *Spacecraft Systems Engineering* (John Wiley & Sons, Ltd, 2003).
10. Willis, P. B. & Hsieh, C. H. Space applications of polymeric materials. *Kobunshi* **49**, 52–56 (2000).
11. Murugesan, S. An overview of electric motors for space applications. *IEEE Trans. Ind. Electron. Control Instrum.* **IECI-28**, 260–265 (1981).
12. Chonis, T. S. et al. Characterization and calibration of the James Webb Space Telescope mirror actuators fine stage motion. In *Space Telescopes and Instrumentation 2018: Optical, Infrared, and Millimeter Wave*. Vol. 10698, 1129 (SPIE, 2018).
13. Scheidler, J., Stalcup, E. & Montbach, E. The impacts of heating actuators in extremely cold space environments. In *IEEE Aerospace Conference Proc*. (IEEE, 2022).
14. Jansson, M., Brizuela, M., Viviente, J. & Merstallinger, A. Harmles – development of dry lubricated harmonic drive gears for space applications. In *Proc. 15th European Space Mechanisms and Tribology Symposium*. 2015 23–25 (Noordwijk: ESA Communications ESTEC, 2015).
15. Sherrit, S. Smart material/actuator needs in extreme environments in space. In *Smart Structures and Materials 2005: Active Materials: Behavior and Mechanics* **5761**, 335 (SPIE, 2005).
16. Carpi, F., Tralli, A., De Rossi, D. & Gaudenzi, P. Martian jumping rover equipped with electroactive polymer actuators: a preliminary study. *IEEE Trans. Aerosp. Electron. Syst.* **43**, 79–92 (2007).
17. Jänker, P. et al. New actuators for aircraft, space and military applications. In *ACTUATOR 2010, 12th International Conference on New Actuators*. 346–354 (WFB, 2008).
18. Mirvakili, S. M. & Hunter, I. W. Artificial muscles: mechanisms, applications, and challenges. *Adv. Mater.* **30**, 1–28 (2018).
19. Riedler, W. et al. MIDAS - The micro-imaging dust analysis system for the Rosetta mission. *Space Sci. Rev.* **128**, 869–904 (2007).
20. Le Letty, R., Barillot, F., Fabbro, H., Guay, P. & Cadiergues, L. *Piezoelectric Actuators for Active Optics* 717–720 (European Space Agency (Special Publ. ESA SP), 2004).
21. Doyon, R. et al. The JWST tunable filter imager (TFI). In *Space Telescopes and Instrumentation 2010: Optical, Infrared, and Millimeter Wave*. Vol. 7731, 77310F (SPIE, 2010).
22. Zanoni, C. & Bortoluzzi, D. Experimental-analytical qualification of a piezoelectric mechanism for a critical space application. *IEEE/ASME Trans. Mechatron.* **20**, 427–437 (2015).
23. Gavrin, A. J., Blizard, K. G., Leo, D. J. & Bennett, M. D. Electroactive smart polymers for space optics. In *Smart Structures and Materials 2004: Smart Structures and Integrated Systems*. Vol. 5390, 217 (SPIE, 2004).
24. Nava, N., Collado, M. & Cabás, R. New pin puller based on SMA technology for space applications. *J. Mater. Eng. Perform.* **23**, 2712–2718 (2014).
25. Guzik, A. & Benafan, O. Design and development of CubeSat solar array deployment mechanisms using shape memory alloys. In *Proc. 44th Aerospace Mechanisms Symposium*. 375–388 (NASA, 2018).
26. Walgren, P. et al. Development and testing of a shape memory alloy-driven composite morphing radiator. *Shape Mem. Superelasticity* **4**, 232–241 (2018).
27. Yamamoto, A. Applications of electrostatic actuators within special environments. In *Next-Generation Actuators Leading Breakthrough*. 363–373 (Springer London, 2010).
28. Pelrine, R., Kornbluh, R., Pei, Q. & Joseph, J. High-speed electrically actuated elastomers with strain greater than 100%. *Science* **287**, 836–839 (2000).
29. Carpi, F. et al. *Electroactive Polymers: New Materials for Spacecraft Structures* 803–816 (European Space Agency (Special Publ. ESA SP, 2005).
30. DeRossi, D. et al. Electro-active polymers for actuation and sensing in space applications. In *International Astronautical Federation - 55th International Astronautical Congress 2004*. Vol. 3, 1991–2001 (AIAA, 2004).
31. Ashby, J., Rosset, S., Henke, E. F. M. & Anderson, I. A. One soft step: bio-inspired artificial muscle mechanisms for space applications. *Front. Robot. AI* **8**, 1–14 (2022).
32. Kornbluh, R. D. et al. Shape control of large lightweight mirrors with dielectric elastomer actuation. In *Smart Structures and Materials 2003: Electroactive Polymer Actuators and Devices (EAPAD)*. Vol. 5051, 143–158 (SPIE, 2003).
33. Menon, C., Carpi, F. & De Rossi, D. Concept design of novel bio-inspired distributed actuators for space applications. *Acta Astronaut.* **65**, 825–833 (2009).
34. Adachi, M., Hamazawa, K., Mimuro, Y. & Kawamoto, H. Vibration transport system for lunar and Martian regolith using dielectric elastomer actuator. *J. Electrostat.* **89**, 88–98 (2017).
35. Araromi, O. A. et al. Rollable multisegment dielectric elastomer minimum energy structures for a deployable microsatellite gripper. *IEEE/ASME Trans. Mechatron.* **20**, 438–446 (2015).
36. Royer, F. et al. Electrostatically actuated thin-shell space structures. In *AIAA SCITECH 2023 Forum*, 1302 (AIAA, 2023).
37. Sîrbu, I. D. et al. Electrostatic actuators with constant force at low power loss using matched dielectrics. *Nat. Electron.* **6**, 888–899 (2023).
38. Acome, E. et al. Hydraulically amplified self-healing electrostatic actuators with muscle-like performance. *Science* **359**, 61–65 (2018).
39. Kellaris, N., Venkata, V. G. opaluni, Smith, G. M., Mitchell, S. K. & Keplinger, C. Peano-HASEL actuators: muscle-mimetic, electrohydraulic transducers that linearly contract on activation. *Sci. Robot.* **3**, eaar3276 (2018).
40. Yoder, Z., Rumley, E. H., Schmidt, I., Rothemund, P. & Keplinger, C. Hexagonal electrohydraulic modules for rapidly speed robots. *Sci. Robot.* **9**, eadl3546 (2024).
41. Sîrbu, I. D. et al. Electrostatic bellow muscle actuators and energy harvesters that stack up. *Sci. Robot.* **6**, 1–12 (2021).
42. Taghavi, M., Helps, T. & Rossiter, J. Electro-ribbon actuators and electro-origami robots. *Sci. Robot.* **3**, eaau9795 (2018).
43. Rothemund, P., Kellaris, N., Mitchell, S. K., Acome, E. & Keplinger, C. HASEL artificial muscles for a new generation of lifelike robots—recent progress and future opportunities. *Adv. Mater.* **2003375**, 1–28 (2020).
44. Moretti, G., Duranti, M., Righi, M., Vertechy, R.& Fontana, M. Analysis of dielectric fluid transducers. in *Electroactive Polymer Actuators and Devices (EAPAD) XX* Vol. 10594 (ed Bar-Cohen, Y.) 29 (SPIE, 2018).
45. Jedynak, L. Vacuum insulation of high voltages utilizing dielectric coated electrodes. *J. Appl. Phys.* **35**, 1727–1733 (1964).
46. Helps, T., Romero, C., Taghavi, M., Conn, A. T. & Rossiter, J. Liquid-amplified zipping actuators for micro-air vehicles with transmission-free flapping. *Sci. Robot.* **7**, 1–14 (2022).
47. Hartmann, F. et al. Highly agile flat swimming robot. *Sci. Robot.* **10**, eadr0721 (2025).
48. Mitchell, S. K. et al. An easy-to-implement toolkit to create versatile and high-performance HASEL actuators for untethered soft robots. *Adv. Sci.* **6**, 1900178 (2019).
49. Jiao, Z., Jiang, L., Sun, J., Huang, J. & Zhu, Y. Outgassing environment of spacecraft: an overview. In *IOP Conference Series: Materials Science and Engineering* Vol. 611 (IOP Publishing, 2019).
50. Cotts, D. B. & Reyes, Z. *New Polymeric Materials Expected to have Superior Properties for Space-based Use*. (SRI Int. Menlo Park. Calif, 1985).
51. Gollor, M. & Rogalla, K. HV design of vacuum-insulated power supplies for space applications. *IEEE Trans. Electr. Insul.* **28**, 667–680 (1993).

52. Young, D. T. et al. Cassini plasma spectrometer investigation. *Space Sci. Rev*. **114**, 1–112 (2004).
53. Mauk, B. H. et al. The energetic particle detector (EPD) investigation and the energetic ion spectrometer (EIS) for the magnetospheric multiscale (MMS) mission. *Space Sci. Rev*. **199**, 471–514 (2016).

Acknowledgements

We thank CCI Eurolam, especially their technical consultant Renato Re for his professionalism and for providing the Pyralux LF adhesive films and the PI/glass fiber laminate.

This research was supported by:
- European Union: NextGenerationEU, PRIN2022 - Progetti di Rilevante Interesse Nazionale, Proj. ZEAP, n. 2022C25PKY, (MF)
- The Italian Ministry of Education, Universities and Research – MUR: *Department of Excellence in Robotics & AI, Scuola Superiore Sant'Anna, Piazza Martiri della Libertà 33, Pisa 56127, Italy* (IDS, MF).
- European Union under ERC Starting Grant, project *flEAP*, grant 101163668 (GM).

Views and opinions expressed are however those of the authors only and do not necessarily reflect those of the European Union, the European Research Council, or the Italian Ministry of Education. Neither the European Union, the Italian Ministry of Education nor the granting authorities can be held responsible for them.

Author contributions

M.F. formulated the goals of this research. M.F., I.-D.S., G.M., D.B., and V.M. planned and coordinated the research activities. M.F. and G.M. acquired the funding. M.F., G.M., D.B., and V.M. supervised the work. I.-D.S. and D.B. developed the vacuum test bench. I.-D.S., A.M., V.M., and G.M. designed and fabricated the actuators. G.M. and I.-D.S. designed and fabricated the compliant gripper. I.-D.S. and U.T. designed the experiments and performed the experimental measurements. I.-D.S., A.M., and U.T. curated the data. I.-D.S. and G.M. wrote the initial paper draft. All authors contributed to reviewing and editing, and accepted the final paper.

Competing interests

The authors declare no competing interests.

Additional information

Supplementary information The online version contains supplementary material available at https://doi.org/10.1038/s41467-025-66232-7.

Correspondence and requests for materials should be addressed to Marco Fontana.

Peer review information *Nature Communications* thanks Florian Hartmann, who co-reviewed with Giulio GrassoQiguang He and the other, anonymous, reviewer for their contribution to the peer review of this work. A peer review file is available.